IEEE Open Journal of the
Industrial Electronics Society

Received 16 November 2021; revised 3 January 2022; accepted 17 January 2022. Date of publication 27 January 2022;
date of current version 9 February 2022. The review of this paper was arranged by Associate Editor Paulo Leitao.

Digital Object Identifier 10.1109/OJIES.2022.3146302

Multi-Agent Position Estimation in Modular Motor Drives Using Low-Resolution Sensors

LYNN VERKROOST [1,2,3], THYMEN VANDENABEELE[1], PETER SERGEANT [1,2] (Senior Member, IEEE), AND HENDRIK VANSOMPEL [1,2]

[1]Electrical Energy Laboratory, Department of Electrical Energy, Metals, Mechanical Constructions and Systems, Ghent University, 9000 Ghent, Belgium
[2]Flanders Make@UGent–EEDT-MP, 3001 Leuven, Belgium
[3]Flanders Make@UGent–EEDT-DC, 3001 Leuven, Belgium

CORRESPONDING AUTHOR: LYNN VERKROOST (e-mail: lynn.verkroost@ugent.be).

The work of Lynn Verkroost was supported by the Research Foundation-Flanders (FWO) through the Ph.D. Fellowship strategic basic research under Project 3S045319. This work is also part of the ModulAr SBO project funded and supported by Flanders Make vzw, the strategic research centre for the manufacturing industry.

ABSTRACT Because a modular motor drive is composed of multiple identical pole drive units and controllers, it can be considered as a multi-agent system. This makes modular motor drives particularly interesting during faults, when the remaining healthy agents assure the continuity of operation. Nevertheless, for some crucial information such as the rotor position, these drives still rely on a single sensor which introduces a single point of failure. In this work, this single high-resolution position sensor is replaced by multiple binary, low-resolution position sensors. A vector tracking observer algorithm, implemented in the different controllers, processes this low-resolution sensor data into a position estimate. Subsequently, these position estimates of the different agents are exchanged with other agents using a distributed averaging algorithm. For this latter approach, it is shown in this work that it improves the position estimation under healthy conditions as well as during agent malfunctions. The concept is demonstrated on a modular axial-flux permanent magnet synchronous machine with fifteen pole drive units, each equipped with a low-resolution position sensor, that are assigned to five agents.

INDEX TERMS Electric motor drives, fault-tolerant, multi-agent system, observer, rotor position.

I. INTRODUCTION

Modular Motor Drives (MMDs) are created by splitting up the Electric Motor (EM) and Power Electronic (PE) converter parts into multiple identical segments [1]. The term pole drive unit is frequently used to indicate a module consisting of an EM and PE segment [2], [3]. Advantages of modular systems include fault tolerance, increased efficiency, better thermal management, power rating scalability, implementation of advanced control strategies, economies of scale, and a possible reduction in the overall size and cost of the PE [4]–[6]. The latter one makes it feasible to integrate the EM and PE into a shared enclosure [7]. This aggressive structural integration results in a fully integrated modular motor drive [8].

To avoid single points of failures, many MMDs also use more than one controller, each driving only a limited set of modules [9]. A choice that is frequently made in literature, is to divide the drive into multiple sets of three pole drive units, and to equip each of these sets with an independent three-phase controller. These so-called multi-three-phase machines can benefit from both the fault tolerance and redundancy of an MMD, while still relying on the well-consolidated three-phase technology [10]–[12].

A modular motor drive in which each set of pole drive units is driven by a separate controller can be considered as a Multi-Agent System (MAS). The agents in such a network can work together to reject disturbances [13], [14], to compensate for failures [15], to perform distributed optimization [16], or, in general, to reach agreement on a specific quantity of interest [17]. The ability of the agents to fuse information of dynamically changing, locally available signals in a decentralized fashion, is commonly referred to as dynamic average consensus [18]. One of its objectives is to obtain higher-accuracy estimates by means of the collective computation of the average of these time-varying signals. The challenge, however,

is that each agent is only capable of local computations, and communication with local neighbors. A variety of methods exists to solve the dynamic average consensus problem, each having their own trade-offs regarding convergence rate, robustness, steady-state error, memory- and communication requirements, noise filtering, and ability to incorporate specific information about the input signals by means of the internal model principle [18], [19].

Modern high-performing motor drives in automotive and industrial processes require a high-resolution rotor position measurement [20]. In some MMDs, a high-resolution encoder or resolver is interfaced with a master controller, that transfers the rotor position to the different controllers that are each driving a set of pole drive units. Since cost and reliability are key parameters, expensive and vulnerable high-resolution encoders or resolvers in these harsh and unfriendly environments are undesirable, as they introduce a single point of failure [21], [22]. Creating redundancy in the mechanical position sensor is also not an option because of its impact on cost and required integration space [23]. Although existing sensorless methods [24]–[28] can be implemented in each of the different controllers in an MMD, the desired performance is not guaranteed within the wide speed and torque range for some mission-critical drives [29].

Inexpensive binary Hall sensors can be combined with estimation algorithms that calculate a high-precision rotor position based on the low-resolution sensor data [30]. Different from the sensorless methods, the estimation is based on discrete absolute rotor position information [31]. Most of these estimation algorithms are based on interpolation techniques [32], Kalman filters [33], [34] or state observers [35]. Despite the use of continuous and differentiable functions that interpolate the quantized discontinuous position in interpolation techniques, time delays and jumps in the rotor position estimate are unavoidable. In Kalman filter based estimation, algorithms usually need to know the noise variance and assume that the quantization error is Gaussian noise, which is not always feasible in practice [29]. State observers combine a high-accuracy and good dynamic characteristics. Nevertheless, the actual performance is heavily influenced by the quality of the observer input and the accuracy of the mechanical model. The quantization of the Hall sensor data generally results in a non-smooth rotor position estimate, and hence, results in torque ripple [36].

In this research, a low-resolution sensor technique is integrated in the multi-agent structure of an MMD. An inexpensive low-resolution sensor is added to each of the pole drive units, and a state-of-the-art state observer is implemented in each of the controllers driving the different sets of pole drive units. Subsequently, the estimated rotor positions of the different agents are shared with the neighbors using a distributed averaging algorithm. It will be demonstrated in this research that this consensus based approach results in a more accurate estimation of the rotor position under normal operation as well as during agent malfunctions. During agent malfunctions, the position estimate of the faulty agent is inherently replaced by the consensus based value of the remaining agents, and hence, the agent can continue its operation.

A proper definition of a pole drive unit, agent, and MMD architecture is given in Section II. In Section III, a state-of-the-art state observer, implemented in the different agents, is discussed. Section IV focuses on the distributed averaging algorithm. Section V finalizes this research with a comprehensive validation on a test setup under healthy operation conditions as well as agent malfunctions.

II. MODULAR MOTOR DRIVE ARCHITECTURE

An overview of the architecture of the modular motor drive is presented in Fig. 1. A motor module consists of a stator core element and a concentrated winding. This motor module is directly connected to a PE module. In this work, the PE module has a half-bridge topology and includes a phase current measurement. A motor module together with a PE module is called a Pole Drive Unit (PDU).

In this work, three of these pole drive units are driven by a standard (micro)controller in which a conventional three-phase field-oriented control algorithm is implemented. The assembly of three pole drive units and one controller is called an agent. The n PDUs in an MMD are hence grouped into $m = n/3$ agents. An agent is a functional entity that can operate independently of the other agents in the system. The agent-specific torque set-points T_i^* ($i \in \{1, \ldots, m\}$) for field-oriented control can be generated by means of a master controller. However, this is not in accordance with the decentralized nature of an MMD. Therefore, ongoing research of the authors is focused on the decentralized distribution of the total torque demand $T_{\text{em}}^* = \sum_i T_i^*$ over the agent-specific set-points T_i^*. However, this research is out of the scope of this paper.

In this research, a low-resolution position sensor is added to each of the pole drive units. As a consequence, each (micro)controller - and hence each agent - receives the digital input of three low-resolution sensors.

Finally, the modular motor drive is composed of multiple agents. A circle communication network is established between the agents. This communication network only allows data exchange with the two closest neighbors of each agent, i.e. agent i can only communicate with agents $i-1$ and $i+1$. The agents use continuous communication, i.e. their communication is time-scheduled. As all the agents are identical, they form a homogeneous communicating MAS.

III. LOW-RESOLUTION POSITION ESTIMATION

As mentioned in the introduction, different types of algorithms exist to turn the low-resolution sensor data into an accurate estimate of the electrical rotor position θ. The algorithm used in this research is adopted from [31], where the Vector Tracking Observer (VTO) presented in Fig. 2 was introduced. Each agent in the MMD uses the binary outputs of its three own low-resolution sensors in its own VTO.

In each agent, the low-resolution sensor data is processed into a spatially rotating vector. This vector moves around the

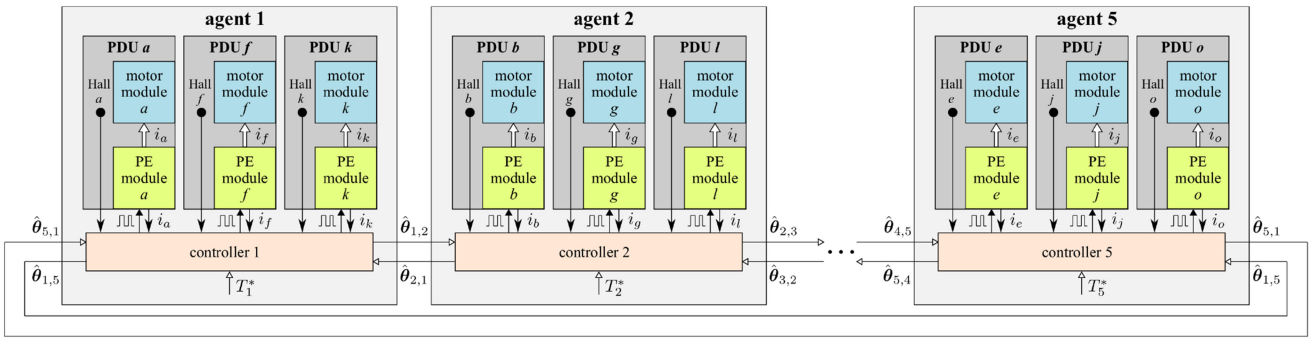

FIGURE 1. Modular motor drive architecture.

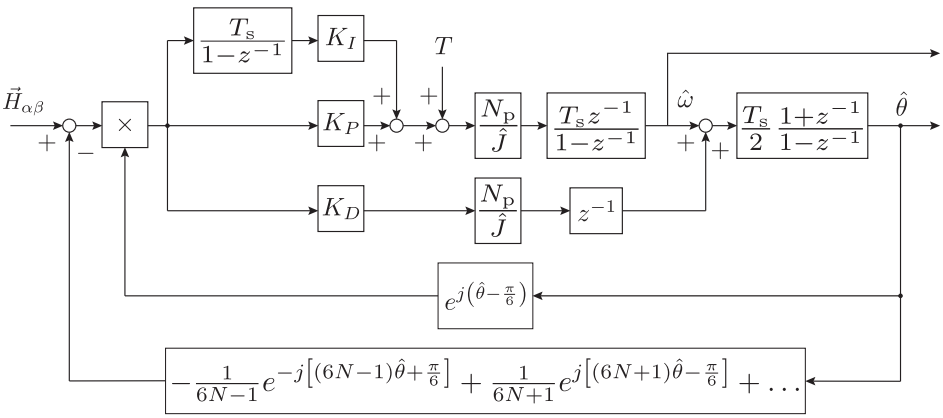

FIGURE 2. Discrete-time vector-tracking observer with decoupling of the spatial harmonic content.

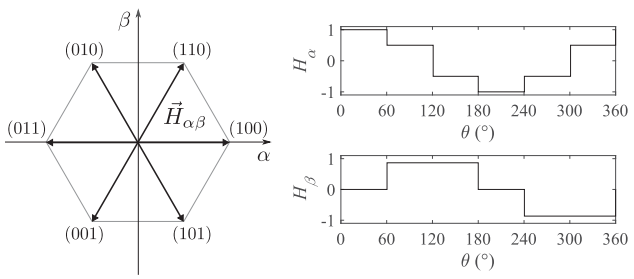

FIGURE 3. The spatially rotating vector $\vec{H}_{\alpha\beta}$ moves around in quantized 60° increments.

hexagon, in quantized 60° increments, as shown in Fig. 3. The spatial harmonic vector $\vec{H}_{\alpha\beta}$ can be expressed as

$$\vec{H}_{\alpha\beta} = e^{j(\theta-\frac{\pi}{6})} + \sum_{N=1}^{+\infty}\left[-\frac{1}{6N-1}e^{-j[(6N-1)\theta+\frac{\pi}{6}]} + \frac{1}{6N+1}e^{j[(6N+1)\theta-\frac{\pi}{6}]}\right] \quad (1)$$

where $e^{j(\theta-\frac{\pi}{6})}$ is the fundamental rotating vector, the remaining terms represent the spatial harmonic content.

Aggressive tuning of the PID-parameters in the VTO in Fig. 2 will result in the tracking of the quantized nature of the input $\vec{H}_{\alpha\beta}$ and will be erroneous. On the other hand, relatively high bandwidth is usually desired in order to obtain a good dynamic estimate of disturbances. To limit the tracking of the quantized nature at low speeds while keeping sufficiently dynamic response at high speeds, the PID-parameters are varied linearly with the rotor speed as suggested in [31].

Also the decoupling of the spatial harmonic content is implemented in the VTO [31]. This results in a rotating vector with strongly reduced quantization harmonic content.

The implementation of the speed dependent gains and decoupling of the spatial harmonic content results in a more or less speed independent error on the electrical position estimate $\hat{\theta}$. Fig. 4 presents the simulated rotor estimate $\hat{\theta}$ and error $\Delta\theta = \hat{\theta} - \theta$ of an agent at a steady-state speed of 500 rpm and a sampling frequency $f_s = 1/T_s$ of 10 kHz. The used PID-parameters have the values $K_P = 71.98$, $K_I = 611.72$ and $K_D = 0.76$ at this rotor speed of 500 rpm. It can be concluded that an agent is capable of estimating the rotor position with sufficiently high accuracy under healthy operation conditions.

Nevertheless, a failing low-resolution sensor (i.e. a sensor whose output is constantly high or low) results in an unusable position estimate, as is illustrated in Fig. 5. If the agent only had this position estimate at its disposal, it would need to be shut down. References [37], [38] explain how such a single sensor fault can be detected by the failing agent itself by the appearance of the zero-vector in the locus of $\vec{H}_{\alpha\beta}$. Also a double sensor fault (i.e. when only one sensor of the agent

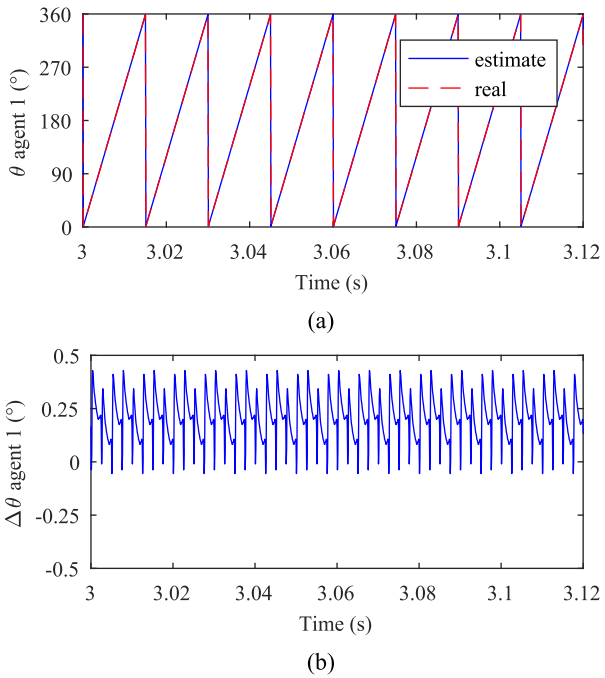

FIGURE 4. Simulated position estimate (a) and error (b) under healthy operation conditions at 500 rpm, based solely on the VTO of a single agent.

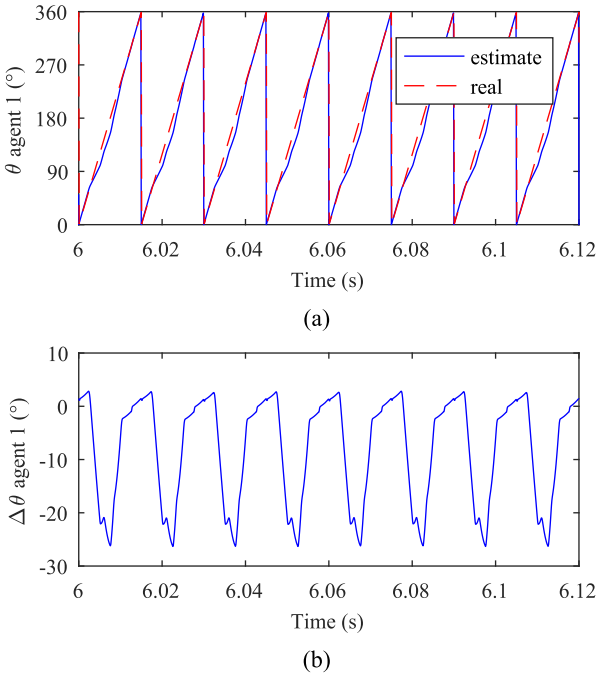

FIGURE 5. Simulated position estimate (a) and error (b) with a single low-resolution sensor malfunction at 500 rpm, based solely on the VTO of the failing agent.

remains functioning properly, and the outputs of the other two sensors are constantly high or low) can be detected by recognizing that only two vectors are switching back and forth. The faulty agent could improve its VTO position estimate by storing specific harmonic decoupling waveforms for every possible fault in look-up tables, which could be accessed once the fault is identified with the method explained in [37]. However, storing these waveforms with an acceptable resolution would require a lot of memory, and the reduced resolution of $\vec{H}_{\alpha\beta}$ would still result in additional ripple in the estimated rotor position [37].

To avoid these disadvantages under sensor malfunctioning, the multi-agent structure of an MMD can be exploited. Since the other agents of the MMD are still healthy, they still have an accurate position estimate available from their VTO. The major contribution of this research is to share this position estimate with the other agents. Sharing the position information will result in an overall better accuracy of the rotor position estimate, and provides an adequate position estimate to the infected agent in post-fault operation without the need to store 18 additional look-up tables in each agent for each of the possible faults. The distributed averaging algorithm that is used for this purpose, is elaborated in Section IV.

IV. DISTRIBUTED AVERAGING ALGORITHM

By establishing communication between the m different agents of the MMD, they can cooperate to further improve their position estimation. Under healthy operation conditions, the distributed computation of a local average increases the accuracy of their estimates, since in the end, all the agents try to estimate the same rotor position. When there is a single or double sensor fault in an agent, both the rotor position estimate $\hat{\theta}$ [el. rad] and the speed estimate $\hat{\omega}$ [el. rad/s] of the VTO of that agent are corrupted. The Distributed Averaging (DA) algorithm presented in this section can provide this faulted agent with an adequate position estimate after the detection of its failure, without the need to change the harmonic decoupling waveforms in its VTO, and without the dissemination of this fault to its neighbors.

To enable the averaging of the discontinuous rotor positions $\theta_i \in [0, 2\pi)$ $(i \in \{1, \ldots, m\})$ of the m agents, these discontinuous signals are transformed into vectors of continuous signals:

$$\boldsymbol{\Theta}_i = [\sin\theta_i \quad \cos\theta_i]^T . \tag{2}$$

As these sine and cosine signals are very fast-varying in time, especially at high rotor speeds, the dynamic consensus algorithms proposed in literature [18], [19] require very high communication rates in order to converge. Therefore, it is opted in this research to use a distributed averaging algorithm that is able to fuse information of five neighboring agents at a communication frequency equal to the sample frequency f_s used for field-oriented control and the VTO. This algorithm does not necessarily converge to the global average of the estimated rotor positions of all the agents in case there are more than five agents, but it is sufficient to provide position estimates with a higher accuracy than the estimates resulting from the VTO of a single agent, and to assure an adequate position estimate in case of a low-resolution sensor malfunction.

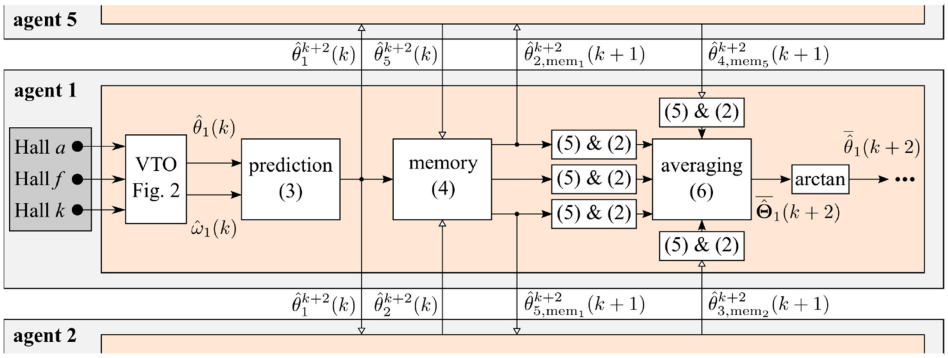

FIGURE 6. Schematic of the distributed averaging algorithm for agent 1.

To compute a local average of the estimated rotor positions $\hat{\theta}_i$ ($i \in \{1, \ldots, m\}$) from the VTOs of the agents, the procedure presented in Fig. 6 is followed. First, the m agents predict their own position estimates for discrete time instant $k+2$, based on the position and speed estimate of their VTO for time instant k:

$$\hat{\theta}_i^{k+2}(k) = \hat{\theta}_i(k) + 2T_s\hat{\omega}_i(k) \tag{3}$$

These predicted position estimates $\hat{\theta}_i^{k+2}(k) \in [0, 2\pi)$ are then exchanged with the two closest neighbors of each agent at time instant $k+1$. When an agent has detected a sensor failure by means of the state-of-the-art fault detection algorithm of [37], it can flag this fault to its neighbors by sending a value that is far outside the normal position range $[0, 2\pi)$.

After this first communication step, each agent i has knowledge about three different position estimates. These three values are stored in the memory of agent i:

$$\hat{\theta}_{i-1,\mathrm{mem}_i}^{k+2}(k+1) = \hat{\theta}_{i-1}^{k+2}(k) \tag{4a}$$

$$\hat{\theta}_{i,\mathrm{mem}_i}^{k+2}(k+1) = \hat{\theta}_{i}^{k+2}(k) \tag{4b}$$

$$\hat{\theta}_{i+1,\mathrm{mem}_i}^{k+2}(k+1) = \hat{\theta}_{i+1}^{k+2}(k) \tag{4c}$$

At time instant $k+2$, a second communication step is conducted. Agent i sends $\hat{\theta}_{i+1,\mathrm{mem}_i}^{k+2}(k+1)$ to agent $i-1$ and $\hat{\theta}_{i-1,\mathrm{mem}_i}^{k+2}(k+1)$ to agent $i+1$, and receives $\hat{\theta}_{i-2,\mathrm{mem}_{i-1}}^{k+2}(k+1) = \hat{\theta}_{i-2}^{k+2}(k)$ from agent $i-1$ and $\hat{\theta}_{i+2,\mathrm{mem}_{i+1}}^{k+2}(k+1) = \hat{\theta}_{i+2}^{k+2}(k)$ from agent $i+1$.

After this second communication step, each agent i has hence knowledge about five different position estimates. For each of these five values $\hat{\theta}_j^{k+2}(k)$ ($j \in \{i-2, i-1, i, i+1, i+2\}$), agent i checks autonomously whether it is a valid position estimate or not:

$$h_j = \begin{cases} 1, & \text{if } \hat{\theta}_j^{k+2}(k) \in [0, 2\pi), \\ 0, & \text{otherwise.} \end{cases} \tag{5}$$

This validity check is required to avoid any negative effect of a failing agent on its healthy neighbors. After all, the objective of the DA algorithm is to improve the rotor position estimates of the agents, and not to spread faults across the whole MMD. The agents do not have to know whether their neighbors make use of their VTO position estimates or not.

After this validity check, the position estimates $\hat{\theta}_j^{k+2}(k)$ are transformed into vectors $\hat{\boldsymbol{\Theta}}_j(k+2)$ of continuous signals according to (2). A local average is then computed based on the known healthy position estimates:

$$\overline{\hat{\boldsymbol{\Theta}}}_i(k+2) = \frac{\sum_j \left[h_j \cdot \hat{\boldsymbol{\Theta}}_j(k+2)\right]}{\sum_j h_j} \tag{6}$$

Eventually, the estimated average rotor position $\overline{\hat{\theta}}_i$ at instant $k+2$ can be recovered from $\overline{\hat{\boldsymbol{\Theta}}}_i(k+2)$ by means of the arctan function. This position estimate $\overline{\hat{\theta}}_i(k+2)$ can then be used in the field-oriented control loop.

In summary, the output of the DA algorithm of agent i at instant $k+2$ (i.e. the estimate $\overline{\hat{\theta}}_i(k+2)$) is based on the outputs of the VTOs of five different agents at instant k. At each time instant, each agent exchanges a vector of two predicted position estimates with each of its two closest neighbors, i.e. it sends the vector

$$\hat{\boldsymbol{\theta}}_{i,i\pm1}(k) = [\hat{\theta}_i^{k+2}(k) \quad \hat{\theta}_{i\mp1,\mathrm{mem}_i}^{k+2}(k)]^T$$

to neighbor $i \pm 1$, and it receives the vector

$$\hat{\boldsymbol{\theta}}_{i\pm1,i}(k) = [\hat{\theta}_{i\pm1}^{k+2}(k) \quad \hat{\theta}_{i\pm2,\mathrm{mem}_{i\pm1}}^{k+2}(k)]^T$$

from that same neighbor. The healthy position estimates are averaged. The prediction step (3) is required to compensate for the time delay of two sample periods T_s introduced by the double communication step.

As the agents do not predict the effects of their actions, but just reactively convert their low-resolution sensor inputs into a position estimate that can be used in a field-oriented control loop, they are reactive agents. They can decide for themselves whether or not to make use of the communicated VTO position estimates of their neighbors based on validity check (5), which makes them autonomous, flexible and communicative. However, the agents cannot change their behavior based on previous experience, so they are non-adaptive.

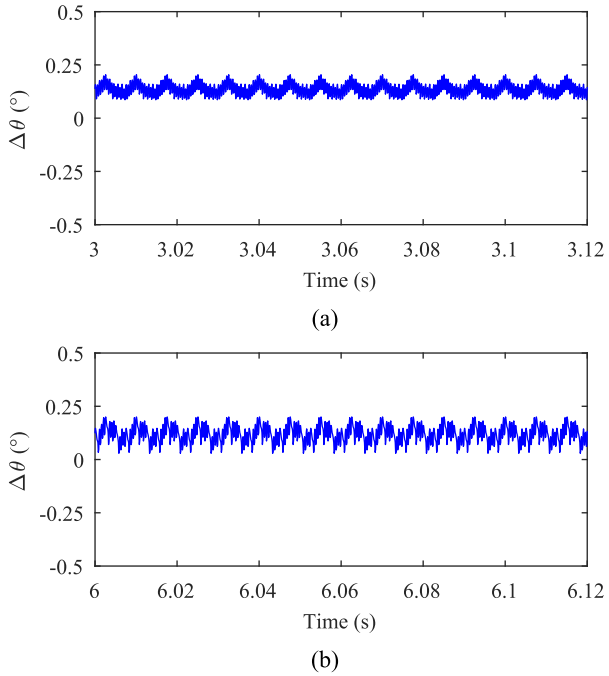

FIGURE 7. Simulated estimation error at 500 rpm after distributed averaging: (a) under healthy operation conditions, (b) with single low-resolution sensor malfunction in agent 1.

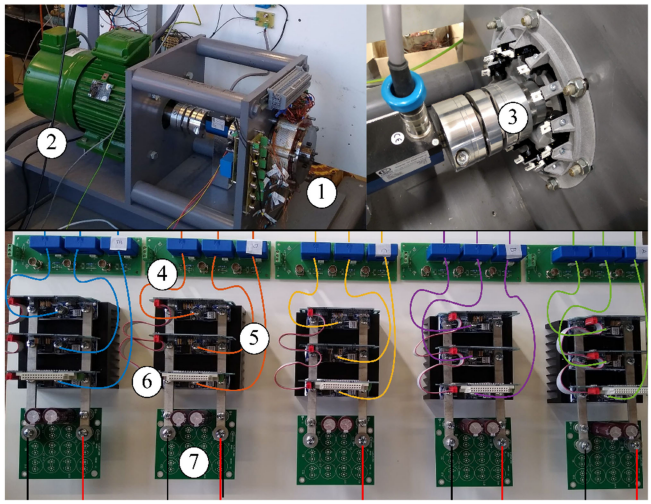

FIGURE 8. Test setup overview: (1) AFPMSM, (2) load motor, (3) low-resolution sensor assembly, (4) phase current measurement, (5) three-phase power module, (6) controller interface, (7) DC-link.

In general, the DA algorithm explained in this section can be adapted to fuse information of x different agents, with x any odd number. This would require the prediction step (3) to change to

$$\hat{\theta}_i^{k+\left(\frac{x-1}{2}\right)}(k) = \hat{\theta}_i(k) + \left(\frac{x-1}{2}\right) T_s \hat{\omega}_i(k) \tag{7}$$

and would involve $(x-1)/2$ communication steps. For instance, if the MMD would comprise only three agents ($m = 3$), only one communication step would be sensible. If the MMD would comprise for instance nine agents ($m = 9$), x could be increased to a value larger than five in order to fuse information of more agents. However, the larger x, the more sensitive the prediction step (7) to speed estimation errors and speed changes, due to the longer prediction horizon and the increased number of sample periods it takes to collect all the required variables by means of neighbor-to-neighbor communication. Therefore, it is advisable to choose $x = 5$, even when $m > 5$, as this choice strikes a good balance between information fusion and robustness.

The modular axial flux PMSM used as case study throughout this work, consists of $n = 15$ pole drive units, grouped into $m = 5$ agents ($n = 3\,m$). The simulation result for this case study under healthy operation conditions is presented in Fig. 7(a). Since the DA algorithm fuses the information of all five agents ($m = 5$ and $x = 5$), the rotor position estimate $\overline{\hat{\theta}}_i$ (and hence the estimation error $\Delta\theta_i = \overline{\hat{\theta}}_i - \theta$) is the same for all five agents $i \in \{1, \ldots, 5\}$. It should be noted, however, that this would not be the case if $m > x$. By comparison with the simulated estimation error presented in Fig. 4(b) for an estimate based solely on the VTO of one agent, it can be concluded that the cooperation between the agents of the MMD by means of the DA algorithm indeed improves the rotor position estimation.

In Fig. 7(b), the simulation results are shown for a single low-resolution sensor malfunction in agent 1: one of its three sensors constantly outputs a low signal. Even under these faulty circumstances, the DA algorithm provides all five agents - including the failing agent - with a position estimate $\overline{\hat{\theta}}$ that has an accuracy comparable to the one under healthy operation conditions presented in Fig. 7(a). Comparison with the outputs of the VTO of one agent only in Figs. 4(b) and 5(b), shows that both the healthy and faulty agents can benefit from the DA algorithm under a sensor malfunction.

V. EXPERIMENTAL VERIFICATION

A. TEST SETUP

In the test setup presented in Fig. 8, a 4 kW Segmented Armature Torus (SAT) Axial-Flux PM Synchronous Machine (AFPMSM), of which the specifications are listed in Table I, is working in motor mode, loaded with an induction motor drive. This AFPMSM is composed of fifteen identical motor modules, of which all thirty power terminals are accessible. The motor modules are connected to a modular low voltage scalable power electronic platform from Infineon. Fig. 8 shows that the power electronics consist of five three-phase power electronic converters, each comprising three identical PE modules that are directly connected to the motor modules of the AFPMSM. Next to the power modules, each agent includes three phase current measurements and three low-resolution sensors. In other words, the test setup comprises fifteen pole drive units, grouped into five agents.

TABLE I Key Specifications of the Segmented Armature Torus AFPMSM

Parameter	Value	Unit
Rated output power	4000	W
Rated speed	2500	rpm
Rated torque T	15	Nm
Rated current	10	A
Number of pole pairs N_{p}	8	-
Slot/tooth number	15	-
Outer diameter housing	195	mm
Outer diameter (active)	148	mm
Inner diameter (active)	100	mm
Axial length stator	61	mm
Total mass	9	kg
Machine inertia J	0.0351	kg·m²
Stator winding resistance $R_{\mathrm{s},i}$ of one agent	65	mΩ
Stator inductance $L_{d,i} = L_{q,i}$ of one agent	309.95	µH
Flux linkage Ψ_d caused by permanent magnets	0.0221	Wb

Binary Hall sensors were not embedded during the construction of the AFPMSM. Therefore, the low-resolution sensors are implemented as through beam photoelectric sensors (EE-SX4009-P1 of Omron) mounted in an assembly as in Fig. 8 at the other side of the flange of the AFPMSM. This assembly consists of a stationary panel, with fifteen photoelectric sensors evenly spaced around the rotating shaft. A disc with eight cutouts is used as an alternative for the magnetic field of the sixteen permanent magnets of the rotor. This disc is mounted on the rotating shaft, and its outer part rotates through the grooves between the emitters and the receivers of the photoelectric sensors. A sensor outputs a low or a high voltage, depending on whether an impermeable part or a cutout of the disc passes through its groove. In this way, the effect of a rotating rotor with eight pole pairs on fifteen Hall sensors embedded in the stator is imitated. The rotor position measurement by the build-in high resolution encoder is referred to as the real rotor position and is not used by the control algorithm.

The position estimation algorithm (the combination of both the VTO and the DA algorithm) is executed at the same frequency as the field-oriented control loop ($f_{\mathrm{s}} = 10$ kHz). In a dSPACE MicroLabBox, the controllers of the five different agents are implemented in five fully independent, parallel blocks. Each block comprises the VTO algorithm of Section III, followed by the DA algorithm of Section IV, in order to process the outputs of three photoelectric sensors into a single high-precision position estimate that can be used for field-oriented control. Both algorithms are executed in one sample period T_{s} of 100 μs. For the DA algorithm, only the communication of the vectors $\hat{\boldsymbol{\theta}}_{i,i\pm1}$ between the neighboring blocks, as depicted in Fig. 1, is allowed.

B. EXPERIMENTAL RESULTS

In Fig. 9(a), the position estimation errors for all the agents without DA (i.e. based on the VTO of each agent only) is presented for a constant speed of 500 rpm. In comparison with the simulated results in Fig. 4(b), it is clear that the error on the measured position estimate is larger. This is due to an

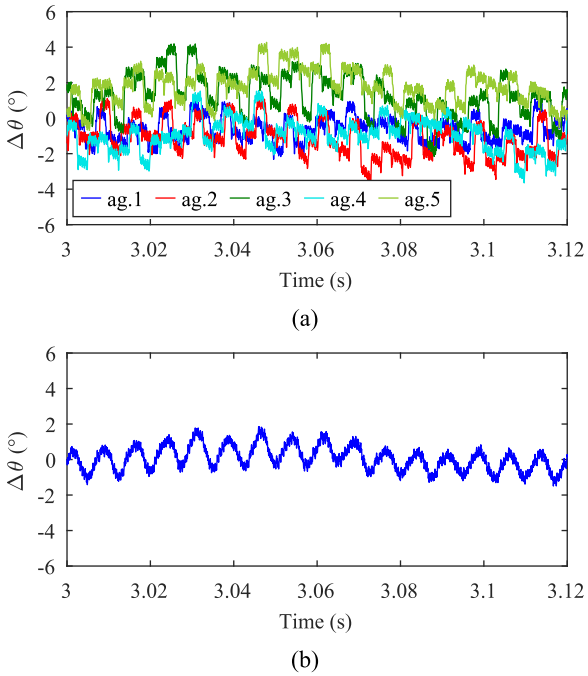

FIGURE 9. Experimental position estimation error at 500 rpm under healthy operation conditions: (a) without DA, (b) with DA.

imperfect positioning of the low-resolution sensors and an unequal width of the rotating disc cutouts due to manufacturing tolerances. As a result, the low-resolution sensor outputs differ from the ideal simulated ones, as is illustrated in Fig. 10. As the look-up tables in the VTOs of the agents are based on the ideal sensor outputs, the discrepancy between these ideal sensor outputs and the real sensor outputs deteriorates the performance of the VTOs. Achieving a good tolerance on the positioning of the low-resolution sensors becomes particular challenging in machines with a high number of pole pairs.

Since the deviation on the positioning of the low-resolution sensors and the width differences of the cutouts in the rotating disc are arbitrary, the DA algorithm results in a slight reduction of the position estimation error, as can be seen in Fig. 9(b).

The measured impact of a single low-resolution sensor fault on the output of the VTO of the faulted agent is shown in Fig. 11(a). The measurement is in good agreement with the simulated results of Fig. 5(b). By using the DA algorithm with $x = m = 5$, all the agents, including the failing one, can be provided with the accurate position estimate shown in Fig. 11(b). Also in this post-fault operation, the position estimate of the agents remains comparable to the one of the healthy system after DA (cfr. Fig. 9(b)), and hence more accurate than the one of the healthy system without DA (cfr. Fig. 9(a)).

Fig. 12 shows the measured position estimation errors under a speed reversal from 500 rpm to -500 rpm with an acceleration of -570 rad/s^2, while a speed step from 1000 rpm to 1500 rpm is imposed in Fig. 13. The measured speed profiles

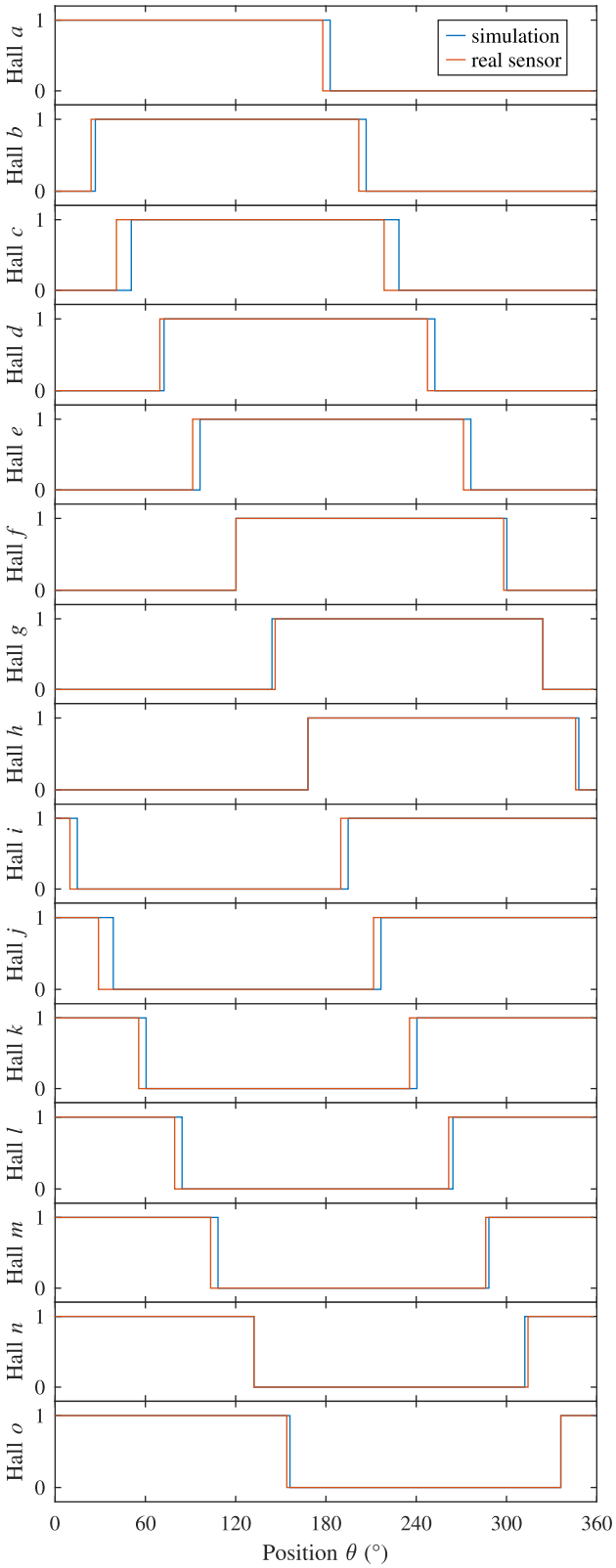

FIGURE 10. **Outputs of the fifteen low-resolution position sensors obtained at a speed of 500 rpm. Hall *x* is the output of the binary sensor of pole drive unit *x*. As a result of the imperfect positioning of the low-resolution sensors and the unequal width of the rotating disc cutouts (both due to manufacturing tolerances), the real sensor outputs differ from the ideal simulated ones.**

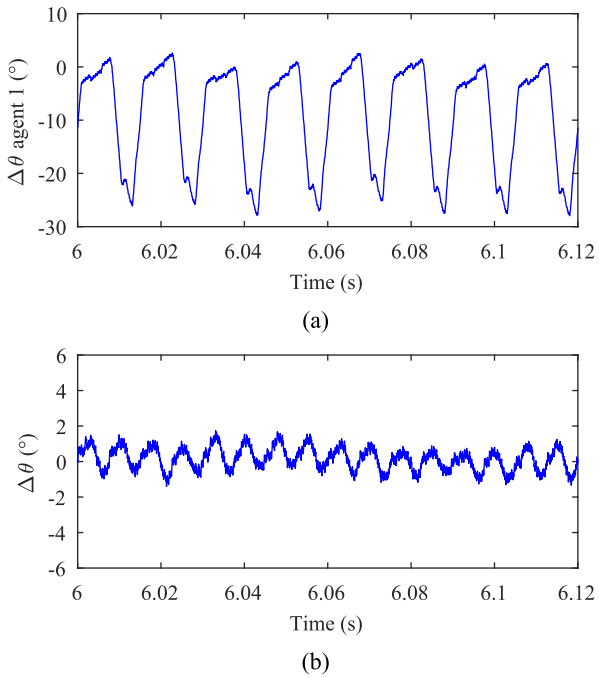

FIGURE 11. **Experimental position estimation error with low-resolution sensor malfunction in agent 1 at 500 rpm: (a) failing agent without DA, (b) all agents with DA.**

in Figs. 12(a) and 13(a) are obtained by means of a high resolution encoder, but are not used by the estimation algorithm. From the comparison of Figs. 12(b) and (c), and 13(b) and (c) can be concluded that the DA algorithm improves the position measurement under these dynamic operation conditions and under these other constant speeds as well. Figs. 12(e) and 13(e) demonstrate once more the ability of the DA algorithm to provide all the agents with an acceptable position estimate under a single low-resolution sensor malfunctioning in agent 1.

The measurements on the test setup hence confirm that the suggested approach results in an accurate rotor position estimation under both normal operation and under a low-resolution sensor failure.

VI. CONCLUSION

In this work, a cheap and fault-tolerant rotor position estimation method applicable to modular motor drives was introduced. In this approach, the modular motor drive was provided with multiple inexpensive, low-resolution position sensors, and was subdivided into different agents. A state-of-the-art vector tracking observer was implemented in each agent, and consequently, a distributed averaging algorithm was added. Both simulations and experiments proved that the rotor position estimate was improved in comparison with the estimation method without the distributed averaging algorithm, under normal operation conditions as well as under sensor malfunctioning.

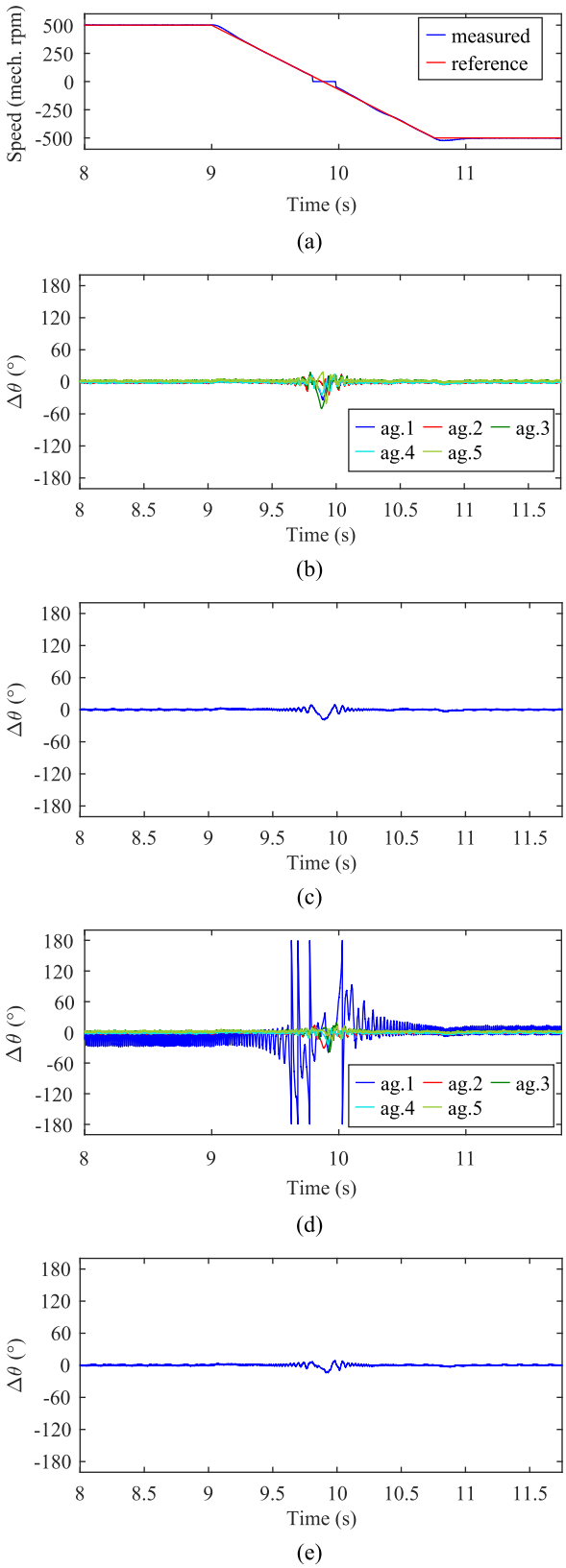

FIGURE 12. Experimental results under the speed reversal depicted in (a): position estimation error, (b) under healthy operation conditions without DA, (c) under healthy operation conditions with DA, (d) with low-resolution sensor malfunction in agent 1 without DA, (e) with low-resolution sensor malfunction in agent 1 with DA.

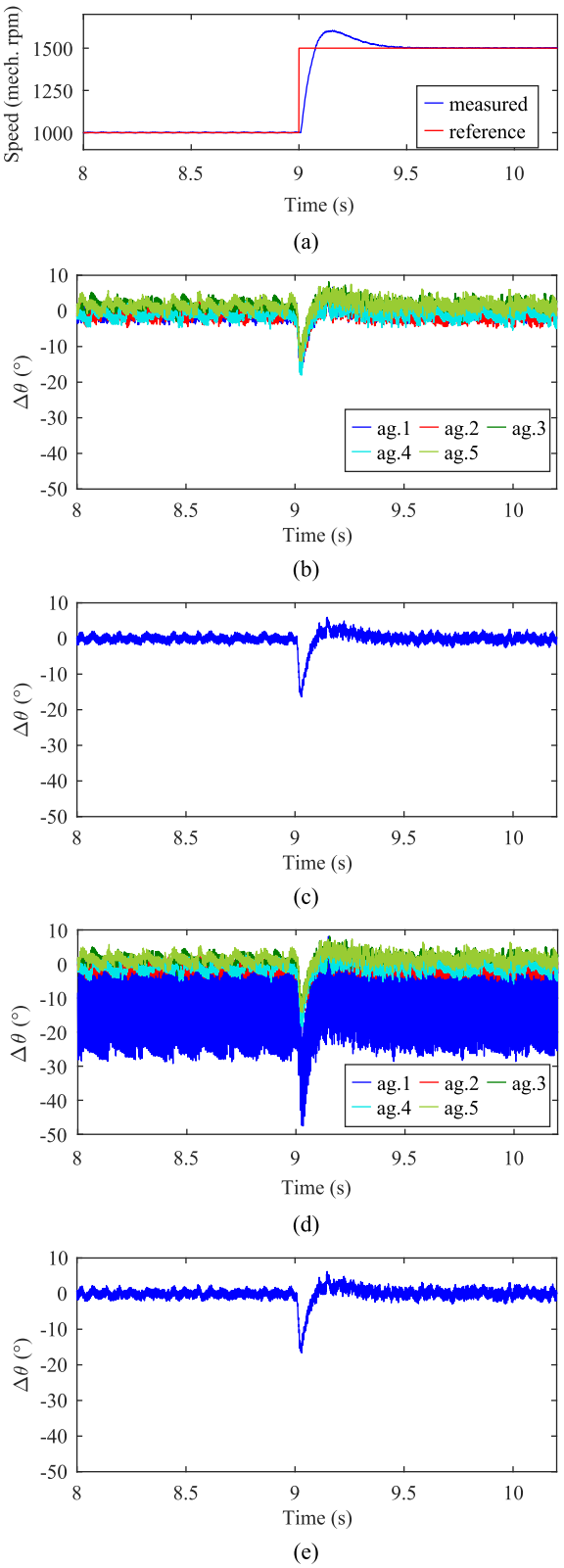

FIGURE 13. Experimental results under the step in speed from 1000 rpm to 1500 rpm depicted in (a): position estimation error, (b) under healthy operation conditions without DA, (c) under healthy operation conditions with DA, (d) with low-resolution sensor malfunction in agent 1 without DA, (e) with low-resolution sensor malfunction in agent 1 with DA.

REFERENCES

[1] M. Uğur, H. Saraç, and O. Keysan, "Comparison of inverter topologies suited for integrated modular motor drive applications," in *Proc. IEEE 18th Int. Power Electron. Motion Control Conf.*, 2018, pp. 524–530, doi: 10.1109/EPEPEMC.2018.8521918.

[2] A. Shea and T. Jahns, "Hardware integration for an integrated modular motor drive including distributed control," in *Proc. IEEE Energy Convers. Congr. Expo.*, 2014, pp. 4881–4887, doi: 10.1109/ECCE.2014.6954070.

[3] M. Uğur and O. Keysan, "Design of a GaN based integrated modular motor drive," in *Proc. 13th Int. Conf. Elect. Machines*, 2018, pp. 1471–1477, doi: 10.1109/ICELMACH.2018.8506862.

[4] R. Abebe *et al.*, "Integrated motor drives: State of the art and future trends," *IET Elect. Power Appl.*, vol. 10, no. 8, pp. 757–771, 2016, doi: 10.1049/iet-epa.2015.0506.

[5] L. Verkroost, J. Van Damme, D. V. Bozalakov, F. De Belie, P. Sergeant, and H. Vansompel, "Simultaneous DC-link and stator current ripple reduction with interleaved carriers in multiphase controlled integrated modular motor drives," *IEEE Trans. Ind. Electron.*, vol. 68, no. 7, pp. 5616–5625, Jul. 2021, doi: 10.1109/TIE.2020.2992965.

[6] M. D. Hennen, M. Niessen, C. Heyers, H. J. Brauer, and R. W. De Doncker, "Development and control of an integrated and distributed inverter for a fault tolerant five-phase switched reluctance traction drive," *IEEE Trans. Power Electron.*, vol. 27, no. 2, pp. 547–554, Feb. 2012, doi: 10.1109/TPEL.2011.2132763.

[7] A. H. R. Mohamed, H. Vansompel, and P. Sergeant, "An integrated modular motor drive with shared cooling for axial flux motor drives," *IEEE Trans. Ind. Electron.*, vol. 68, no. 11, pp. 10467–10476, Nov. 2022, doi: 10.1109/TIE.2020.3028818.

[8] A. H. Mohamed, H. Vansompel, and P. Sergeant, "Design of an integrated DC-link structure for reconfigurable integrated modular motor drives," *IEEE Trans. Ind. Electron.*, vol. 69, no. 3, pp. 2312–2321, Mar. 2022, doi: 10.1109/TIE.2021.3065620.

[9] J. Wang, Y. Li, and Y. Han, "Integrated modular motor drive design with GaN power FETs," *IEEE Trans. Ind. Appl.*, vol. 51, no. 4, pp. 3198–3207, Jul./Aug. 2015, doi: 10.1109/TIA.2015.2413380.

[10] E. Prieto-Araujo, A. Junyent-Ferré, D. Lavèrnia-Ferrer, and O. Gomis-Bellmunt, "Decentralized control of a nine-phase permanent magnet generator for offshore wind turbines," *IEEE Trans. Energy Convers.*, vol. 30, no. 3, pp. 1103–1112, 2015, doi: 10.1109/TEC.2015.2412550.

[11] M. J. Duran and F. Barrero, "Recent advances in the design, modeling, and control of multiphase machines—Part II," *IEEE Trans. Ind. Electron.*, vol. 63, no. 1, pp. 459–468, Jan. 2016, doi: 10.1109/TIE.2015.2448211.

[12] S. Rubino, O. Dordevic, R. Bojoi, and E. Levi, "Modular vector control of multi-three-phase permanent magnet synchronous motors," *IEEE Trans. Ind. Electron.*, vol. 68, no. 10, pp. 9136–9147, Oct. 2021, doi: 10.1109/TIE.2020.3026271.

[13] Z. Ding, "Consensus disturbance rejection with disturbance observers," *IEEE Trans. Ind. Electron.*, vol. 62, no. 9, pp. 5829–5837, Sep. 2015, doi: 10.1109/TIE.2015.2442218.

[14] D. Meng and Y. Jia, "Robust consensus algorithms for multiscale coordination control of multivehicle systems with disturbances," *IEEE Trans. Ind. Electron.*, vol. 63, no. 2, pp. 1107–1119, Feb. 2016, doi: 10.1109/TIE.2015.2478740.

[15] Y. Wang, Y. Song, and F. L. Lewis, "Robust adaptive fault-tolerant control of multiagent systems with uncertain nonidentical dynamics and undetectable actuation failures," *IEEE Trans. Ind. Electron.*, vol. 62, no. 6, pp. 3978–3988, Jun. 2015, doi: 10.1109/TIE.2015.2399400.

[16] M. H. Ullah, B. Babaiahgari, A. Alseyat, and J.-D. Park, "A computationally efficient consensus-based multiagent distributed EMS for DC microgrids," *IEEE Trans. Ind. Electron.*, vol. 68, no. 6, pp. 5425–5435, Jun. 2021, doi: 10.1109/TIE.2020.2992015.

[17] J. Qin, Q. Ma, Y. Shi, and L. Wang, "Recent advances in consensus of multi-agent systems: A brief survey," *IEEE Trans. Ind. Electron.*, vol. 64, no. 6, pp. 4972–4983, Jun. 2017, doi: 10.1109/TIE.2016.2636810.

[18] S. S. Kia, B. Van Scoy, J. Cortes, R. A. Freeman, K. M. Lynch, and S. Martinez, "Tutorial on dynamic average consensus: The problem, its applications, and the algorithms," *IEEE Control Syst. Mag.*, vol. 39, no. 3, pp. 40–72, Jun. 2019, doi: 10.1109/MCS.2019.2900783.

[19] H. Bai, R. A. Freeman, and K. M. Lynch, "Robust dynamic average consensus of time-varying inputs," in *Proc. 49th IEEE Conf. Decis. Control*, 2010, pp. 3104–3109, doi: 10.1109/CDC.2010.5717485.

[20] K. Scicluna, C. S. Staines, and R. Raute, "Sensorless low/zero speed estimation for permanent magnet synchronous machine using a search-based real-time commissioning method," *IEEE Trans. Ind. Electron.*, vol. 67, no. 7, pp. 6010–6018, Jul. 2020, doi: 10.1109/TIE.2020.2965483.

[21] J. Xu, Y. Du, H. Fang, H. Guo, and Y.-H. Chen, "A robust observer and nonorthogonal PLL-based sensorless control for fault-tolerant permanent magnet motor with guaranteed postfault performance," *IEEE Trans. Ind. Electron.*, vol. 67, no. 7, pp. 5959–5970, Jul. 2020, doi: 10.1109/TIE.2019.2931235.

[22] L. Ding, Y. W. Li, and N. R. Zargari, "Discrete-time SMO sensorless control of current source converter-fed PMSM drives with low switching frequency," *IEEE Trans. Ind. Electron.*, vol. 68, no. 3, pp. 2120–2129, Mar. 2021, doi: 10.1109/TIE.2020.2972433.

[23] J. Xu, Y. Du, B. Zhang, H. Fang, H. Guo, and Y.-H. Chen, "Sensorless fault tolerant control with phase delay compensation for aerospace FTPMSM drives with phase open-circuit and short-circuit faults," *IEEE Trans. Ind. Electron.*, vol. 68, no. 6, pp. 4576–4585, Jun. 2021, doi: 10.1109/TIE.2020.2988231.

[24] G. Wang, M. Valla, and J. Solsona, "Position sensorless permanent magnet synchronous machine drives—A review," *IEEE Trans. Ind. Electron.*, vol. 67, no. 7, pp. 5830–5842, Jul. 2020, doi: 10.1109/TIE.2019.2955409.

[25] C. J. V. Filho, D. Xiao, R. P. Vieira, and A. Emadi, "Observers for high-speed sensorless PMSM drives: Design methods, tuning challenges and future trends," *IEEE Access*, vol. 9, pp. 56 397–56 415, 2021, doi: 10.1109/ACCESS.2021.3072360.

[26] Y. Zhang, Z. Yin, C. Bai, G. Wang, and J. Liu, "A rotor position and speed estimation method using an improved linear extended state observer for IPMSM sensorless drives," *IEEE Trans. Power Electron.*, vol. 36, no. 12, pp. 14 062–14 073, Dec. 2021, doi: 10.1109/TPEL.2021.3085126.

[27] C. Wu, Z. Chen, and Q. Chen, "An optimized asymmetric pulsewidth modulation for sensorless control of permanent magnet synchronous machines," *IEEE Trans. Ind. Electron.*, vol. 69, no. 2, pp. 1389–1399, Feb. 2022, doi: 10.1109/TIE.2021.3060676.

[28] V. Repecho, J. B. Waqar, D. Biel, and A. Dòria-Cerezo, "Zero speed sensorless scheme for permanent magnet synchronous machine under decoupled sliding-mode control," *IEEE Trans. Ind. Electron.*, vol. 69, no. 2, pp. 1288–1297, Feb. 2022, doi: 10.1109/TIE.2021.3062260.

[29] Q. Ni *et al.*, "A new position and speed estimation scheme for position control of PMSM drives using low-resolution position sensors," *IEEE Trans. Ind. Appl.*, vol. 55, no. 4, pp. 3747–3758, Jul./Aug. 2019, doi: 10.1109/TIA.2019.2904934.

[30] S. Zaim, J. Martin, B. Nahid-Mobarakeh, and F. Meibody-Tabar, "High performance low cost control of a permanent magnet wheel motor using a hall effect position sensor," in *Proc. IEEE Veh. Power Propulsion Conf.*, 2011, pp. 1–6, doi: 10.1109/VPPC.2011.6043245.

[31] M. C. Harke, G. De Donato, F. G. Capponi, T. R. Tesch, and R. D. Lorenz, "Implementation issues and performance evaluation of sinusoidal, surface-mounted PM machine drives with hall-effect position sensors and a vector-tracking observer," *IEEE Trans. Ind. Appl.*, vol. 44, no. 1, pp. 161–173, Jan./Feb. 2008, doi: 10.1109/TIA.2007.912729.

[32] Z. Feng and P. P. Acarnley, "Extrapolation technique for improving the effective resolution of position encoders in permanent-magnet motor drives," *IEEE/ASME Trans. Mechatronics*, vol. 13, no. 4, pp. 410–415, Aug. 2008, doi: 10.1109/TMECH.2008.2001689

[33] J. Kim and B. K. Kim, "Development of precise encoder edge-based state estimation for motors," *IEEE Trans. Ind. Electron.*, vol. 63, no. 6, pp. 3648–3655, Jun. 2016, doi: 10.1109/TIE.2016.2539249.

[34] B. Han, Y. Shi, and H. Li, "Position estimation for ultra-low speed gimbal servo system of SGMSCMG based on linear hall sensors," *IEEE Sensors J.*, vol. 20, no. 20, pp. 12 174–12 183, Oct. 2020, doi: 10.1109/JSEN.2020.2999781.

[35] S.-Y. Kim, C. Choi, K. Lee, and W. Lee, "An improved rotor position estimation with vector-tracking observer in PMSM drives with low-resolution hall-effect sensors," *IEEE Trans. Ind. Electron.*, vol. 58, no. 9, pp. 4078–4086, Sep. 2011, doi: 10.1109/TIE.2010.2098367.

[36] F. G. Capponi, G. De Donato, L. Del Ferraro, O. Honorati, M. C. Harke, and R. D. Lorenz, "AC brushless drive with low-resolution hall-effect sensors for surface-mounted PM machines," *IEEE Trans. Ind. Appl.*, vol. 42, no. 2, pp. 526–535, Mar./Apr. 2006, doi: 10.1109/TIA.2005.863904.

[37] G. Scelba, G. De Donato, G. Scarcella, F. Giulii Capponi, and F. Bonaccorso, "Fault-tolerant rotor position and velocity estimation using binary hall-effect sensors for low-cost vector control drives," *IEEE Trans. Ind. Appl.*, vol. 50, no. 5, pp. 3403–3413, Sep./Oct. 2014, doi: 10.1109/TIA.2014.2304616.

[38] G. Scelba, G. De Donato, M. Pulvirenti, F. Giulii Capponi, and G. Scarcella, "Hall-effect sensor fault detection, identification, and compensation in brushless DC drives," *IEEE Trans. Ind. Appl.*, vol. 52, no. 2, pp. 1542–1554, Mar./Apr. 2016, doi: 10.1109/TIA.2015.2506139.

LYNN VERKROOST was born in Belgium, in 1994. She received the M.Sc. degree in electromechanical engineering from Ghent University, Ghent, Belgium, in 2017. Since 2017, she has been with the Electrical Energy Laboratory, Department of Electromechanical, Systems and Metal Engineering, Ghent University, where she is currently working toward the Ph.D. degree in electromechanical engineering. She is an Affiliate Member of Flanders Make, the strategic research center for the manufacturing industry in Flanders, Belgium. Her current research interests include digital, fault tolerant, and distributed control of converter-fed electrical machines.

Verkroost received a Ph.D. fellowship from Research Foundation-Flanders in 2019.

THYMEN VANDENABEELE was born in Belgium, in 1998. He received the M.Sc. degree in electrical power engineering from Ghent University, Ghent, Belgium, in 2021. His research interests include electrical power engineering and position estimation in modular motor drives.

PETER SERGEANT (Senior Member, IEEE) was born in Belgium, in 1978. He received the M.Sc. and Ph.D. degrees in electromechanical engineering from Ghent University, Ghent, Belgium, in 2001 and 2006, respectively. He was a Postdoctoral Fellow with Research Foundation - Flanders and in 2006, he became a Postdoctoral Researcher with Ghent University. Since 2012, he has been an Associate Professor with Ghent University. He is also a Core Lab Manager in the cluster Motion Products of Flanders Make. His current research interests include electrical machines and drives for industrial and for sustainable energy applications, accurate computation of losses in machines and drives, improving energy efficiency, and increasing power density.

HENDRIK VANSOMPEL was born in Belgium, in 1986. He received the M.Sc. and Ph.D. degrees in electromechanical engineering from Ghent University, Ghent, Belgium, in 2009 and 2013, respectively. He is currently a Postdoctoral Research Assistant and an Associate Professor with the Department of Electromechanical, Systems and Metal Engineering, Ghent University. He is an Affiliate Member of Flanders Make, the strategic research center for the manufacturing industry in Flanders, Belgium. His research interests include electric machines and power electronics.